RESEARCH ARTICLE

JOR *Spine* OPEN ACCESS

Facet deflection and strain are dependent on axial compression and distraction in C5–C7 spinal segments under constrained flexion

Parham Foroutan[1,2] | Ryan D. Quarrington[1,2,3] | Michael Pyrros Russo[4] |
Boyin Ding[1] | Peter A. Cripton[5] | John J. Costi[4] | Claire F. Jones[1,2,6]

[1]School of Electrical and Mechanical Engineering, The University of Adelaide, Adelaide, South Australia, Australia

[2]Adelaide Spinal Research Group, Centre for Orthopaedic & Trauma Research, Faculty of Health and Medical Sciences, The University of Adelaide, Adelaide, South Australia, Australia

[3]Adelaide Medical School, The University of Adelaide, Adelaide, South Australia, Australia

[4]Biomechanics and Implants Research Group, Medical Device Research Institute, College of Science and Engineering, Flinders University, Adelaide, South Australia, Australia

[5]Orthopaedic and Injury Biomechanics Group, School of Biomedical Engineering and Departments of Mechanical Engineering and Orthopaedics, University of British Columbia, Vancouver, British Columbia, Canada

[6]Department of Orthopaedics & Trauma, Royal Adelaide Hospital, Adelaide, South Australia, Australia

Correspondence
Claire F. Jones, School of Electrical and Mechanical Engineering, The University of Adelaide, Level 7, Adelaide Health and Medical Sciences Building, North Terrace, Adelaide, SA 5000, Australia.
Email: claire.jones@adelaide.edu.au

Abstract

Background: Facet fractures are frequently associated with clinically observed cervical facet dislocations (CFDs); however, to date there has only been one experimental study, using functional spinal units (FSUs), which has systematically produced CFD with concomitant facet fracture. The role of axial compression and distraction on the mechanical response of the cervical facets under intervertebral motions associated with CFD in FSUs has previously been shown. The same has not been demonstrated in multi-segment lower cervical spine specimens under flexion loading (postulated to be the local injury vector associated with CFD).

Methods: This study investigated the mechanical response of the bilateral inferior C6 facets of thirteen C5-C7 specimens (67±13 yr, 6 male) during non-destructive constrained flexion, superimposed with each of five axial conditions: (1) 50 N compression (simulating weight of the head); (2-4) 300, 500, and 1000 N compression (simulating the spectrum of intervertebral compression resulting from neck muscle bracing prior to head-first impact and/or externally applied compressive forces); and, (5) 2 mm of C6/C7 distraction (simulating the intervertebral distraction present during inertial loading of the cervical spine by the weight of the head). Linear mixed-effects models ($\alpha = 0.05$) assessed the effect of axial condition.

Results: Increasing amounts of intervertebral compression superimposed on flexion rotations, resulted in increased facet surface strains (range of estimated mean difference relative to Neutral: *maximum principal* = 77 to 110 $\mu\varepsilon$, *minimum principal* = 126 to 293 $\mu\varepsilon$, *maximum shear* = 203 to 375 $\mu\varepsilon$) and angular deflection of the bilateral inferior C6 facets relative to the C6 vertebral body (range of estimated mean difference relative to Neutral = 0.59° to 1.47°).

Conclusions: These findings suggest increased facet engagement and higher load transfer through the facet joint, and potentially a higher likelihood of facet fracture under the compressed axial conditions.

1 | INTRODUCTION

Cervical facet dislocations (CFD) are, by virtue of their frequent association with severe spinal cord injury, one of the most debilitating spinal injuries. The most common causes of CFDs are motor vehicle crashes, sporting accidents, and falls.[1–4] They present most frequently at the C5/C6 and C6/C7 spinal levels,[3,5,6] and are associated with fracture of the facets in up to 70% of clinical cases.[3,7] The mechanism of CFD is not fully understood; however, previous ex vivo studies have suggested that the injury results from axial compressive forces applied cranially with large anterior eccentricity during simulated head-first impact,[8–10] or from inertial loading of the spine by the weight of the head during high deceleration events.[11–15] Applying a *global* eccentric axial compressive force to whole cervical spines ex vivo, has been shown to result in the extension of the upper-to-middle, and flexion of the middle-to-lower, cervical spine.[16–18] The *local* flexion moment imposed on the lower cervical spine, where CFDs are most frequently seen, is thought to produce *intervertebral* anterior shear and flexion motions at the level of dislocation.[19–21] Inertially produced CFDs ex vivo have only been demonstrated in functional spinal units (FSUs); flexion, anterior shear, and distraction at the level of dislocation have been reported as the predominant sagittal plane *intervertebral* motions.[12]

Facet fractures are frequently associated with clinically observed CFDs; however, to date there has only been one experimental study, using C6/C7 FSUs, which has reported CFD with concomitant facet fracture (CFD + Fx).[21] In a review of 170 head-first impact configuration tests of whole cadavers, full head–neck specimens, full osteoligamentous cervical spines (C1–T1), and any five (or more) consecutive-vertebra spinal segments (e.g., C3–C7), only 19 CFDs and no CFD + Fx were identified.[22,23] The scarcity of facet fractures in the experimental literature, at both quasistatic and dynamic loading rates, may be due to inadequate replication of the complex loading patterns and muscle forces present in in vivo injury scenarios. To elucidate the loading patterns most likely to result in facet fractures concomitant to CFD, an understanding of the mechanical response of the cervical facets to the *intervertebral*, *local*, and *global* motions associated with the injury is required.

A number of studies have investigated the individual and combined effect/s of *intervertebral* motions thought to be associated with CFD on the mechanical response of the cervical facets in FSUs. The angular deflection, surface strain, stiffness, and failure load of isolated sub-axial cervical facets, under simulated flexion and anterior shear loading have been quantified.[24] Facet deflections and surface strains under non-destructive anterior shear, flexion, lateral bending, and axial rotation loading of lower cervical FSUs have also been reported.[23,25] Nightingale et al.[26] reported that including muscle loads (either passive or active) in computational simulations of head-first

impact substantially increased intervertebral compressive and shear loads compared with simulations without muscle loads. Superimposing intervertebral axial *compression* (which could result from neck muscle bracing before head-first impact, and/or externally applied compressive forces) or *distraction* (which could result from inertial loading of the cervical spine by the weight of the head, such as in a restrained occupant in a frontal collision) on intervertebral anterior shear and flexion motions has been shown to affect the mechanical response of the facets in lower cervical FSUs. Using C6/C7 FSUs, Quarrington et al.[23] showed that minimum principal and maximum shear strains, and angular deflection of the bilateral inferior C6 facets relative to the C6 vertebral body (VB), were significantly higher when intervertebral axial compression rather than distraction was superimposed on non-destructive flexion motions. Increased facet engagement, as indicated by greater facet deflections and maximum shear strains at the facet bases, have also been reported in C6/C7 FSUs subjected to constrained anterior shear loading superimposed with axial compression compared with distraction.[21]

Although these studies have highlighted the role of axial compression and distraction on the mechanical response of the facets under *intervertebral* motions associated with CFD in FSUs, the same has not been demonstrated in multisegment lower cervical spine specimens under *local* flexion loading. The current study aims to investigate the effect of five varying axial conditions on the sagittal angular deflection and surface strains of the bilateral inferior C6 facets of C5–C7 spinal segments subjected to non-destructive constrained flexion (postulated to be the *local* injury vector associated with CFD[19,20]).

2 | METHODS

2.1 | Specimen preparation

This study was approved by the University of Adelaide Institutional Human Research Ethics Committee (H-2018-261). Thirteen C5–C7 spinal segments were dissected from fresh-frozen (−20°C) human cervical spines (67 ± 13 year, 6 male). Computed tomography (CT) scans (SOMATOM Force, Siemens, Erlangen, Germany; $0.23 \times 0.23 \times 0.4$ mm voxel size) were obtained and reviewed to ensure specimens had no prior surgical interventions to the head or spine, and had no fusion or osteophytes associated with the intervertebral disc or facet joints that could limit motion. Musculature and associated soft tissue were removed, leaving the intervertebral discs, ligaments, and facet joint capsules intact. The C5 and C7 vertebral bodies were augmented with screws and wire, and sequentially embedded into aluminum potting cups using polymethylmethacrylate (PMMA, Vertex Dental, Utrecht, The Netherlands). The C7 vertebra was embedded first, with the most anterior point of the neural canal

FIGURE 1 (A) Schematic showing a sagittal view of an embedded specimen, with the most anterior point of the spinal canal aligned with the mid-coronal plane of the potting cup, and the mid-transverse plane of the C6/C7 disc aligned horizontally. (B) Schematic showing a frontal view of an embedded specimen, with the midsagittal plane of the specimen aligned with that of the potting cup. (C) 3D reconstruction of CT scan of a potted C5–C7 specimen. Schematics not to scale. The curvature of the C5–C7 segment in the sagittal plane (A) has been exaggerated to highlight the alignment of the C6/C7 mid-transverse plane.
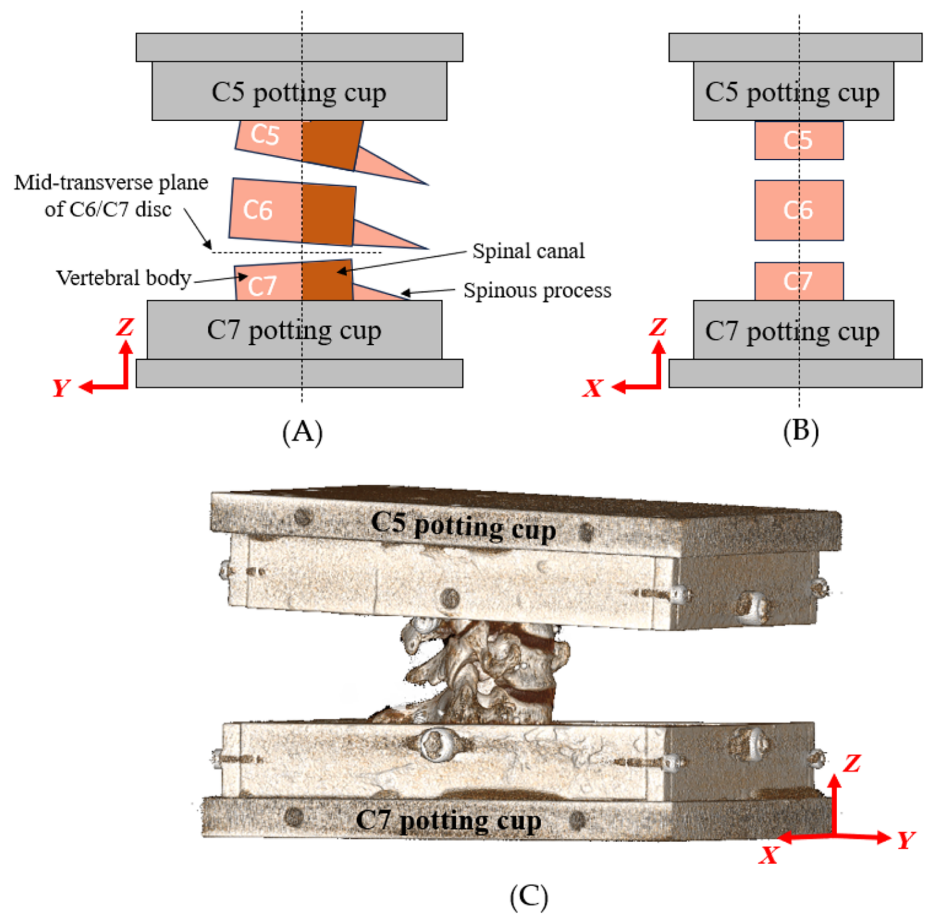
aligned with the mid-coronal plane of the potting cup (Figure 1A), the midsagittal plane of the specimen aligned with that of the potting cup (Figure 1B), and the mid-transverse plane of the C6/C7 disc aligned horizontally (Figure 1A). The superior and inferior potting cups were then placed in a custom alignment jig which ensured the corresponding faces of the superior and inferior potting cups were parallel; subsequently, the C5 vertebra was embedded in PMMA. The mediolateral and anterior–posterior (AP) center of the C6/C7 disc were located using the corners of the inferior C6 and superior C7 endplate in AP and lateral radiographs of embedded specimens. Offsets from the center of the C6/C7 disc to the center of the C5 potting cup were then calculated and used to mechanically prescribe the center of the C6/C7 disc as the fixed center of rotation (CoR)[27–29] for flexion rotation during mechanical testing. Throughout the preparation and mechanical testing, specimen hydration was maintained by intermittent spraying of phosphate-buffered saline (PBS).

2.2 | Mechanical testing apparatus

The specimen-PMMA assembly was mounted in the workspace of a custom-built six degree-of-freedom Hexapod robot,[30] aligned with the robot's global coordinate system (+X = right lateral, +Y = anterior, +Z = cranial). Briefly, the Hexapod robot is a modified Stewart platform and employs six servocontrolled ball screw-driven
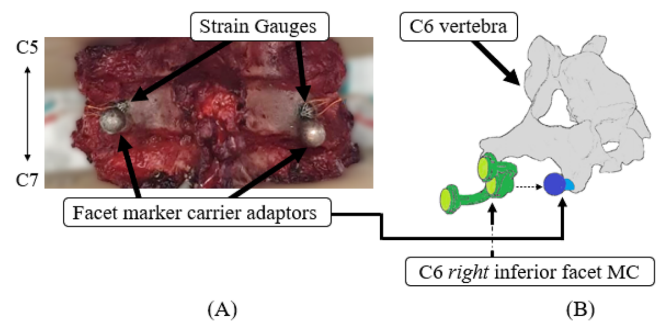
FIGURE 2 (A) Posterior view of a potted C5–C7 specimen, showing facet MC adaptors attached to the tip of the bilateral inferior C6 facets, and strain gauges attached superior-medially to the facet MC adaptors. (B) Schematic illustrating how the facet MCs (green) attach to the facet MC adaptors (dark blue sphere, light blue cylindrical support).

linear actuators to position a mobile end effector with respect to a stationary base plate. Specimens are fixed between the stationary base and the mobile end effector. Load cells attached to the base and end effector were used to obtain superior and inferior loads, respectively. Due to the limited stroke length of the linear actuators, the robot is capable of 20°–24° of flexion rotation, depending on specimen height and the CoR. The translational and rotational accuracy of the robot, in the configuration used for this study, are 0.1 mm and 0.2°, respectively.

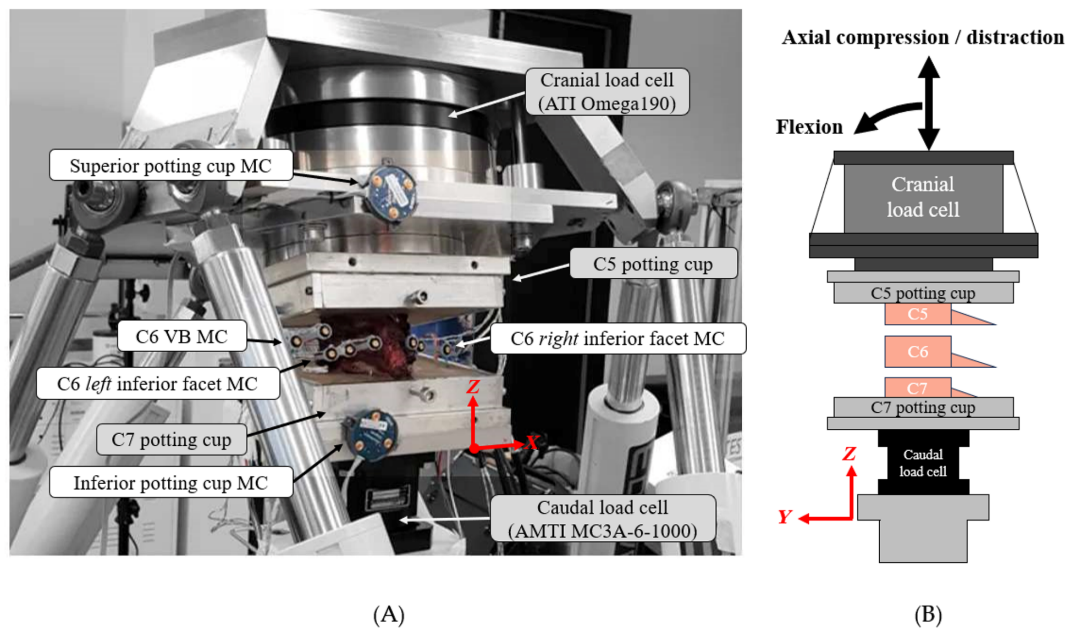**FIGURE 3** (A) Posterolateral view of the potted C5–C7 specimen fixed between the caudal (fixed) and cranial (rotating with end effector) load cells. The motion capture MCs attached to the C6 VB, the C6 left and right inferior facets, and the superior and inferior potting cups are shown. (B) A simplified schematic of the testing assembly (sagittal view), depicting the specimen fixed in the workspace of the hexapod, and highlighting the motions applied by the end effector (flexion, axial compression/distraction).

2.3 | Instrumentation and data collection

A custom lightweight facet marker carrier (MC) adaptor was glued to the tip of the bilateral inferior C6 facets using cyanoacrylate adhesive (Loctite 401, Henkel, Düsseldorf, Germany) (Figure 2A), and a motion capture MC (custom-built using three non-collinear small diameter infrared emitting diodes, Northern Digital Inc., Ontario, Canada) was attached to each adaptor (Figures 2B and 3A). An MC was also attached to the C6 VB using a K-wire inserted <5 mm into the trabecular bone (Figure 3A). The MCs attached to the C6 VB and inferior facets were used to measure the angular deflection of the inferior C6 facets relative to the C6 VB. A triaxial strain gauge (FRA-1-23-1L, TML, Tokyo, Japan) was glued superior-medially to the facet MC adaptor on each of the inferior C6 facets, to measure facet surface strains (Figure 2A). A motion capture MC (smart marker rigid body, Northern Digital Inc., Ontario, Canada) was attached to the superior potting cup to measure the translations and rotations of the hexapod end effector, and to the inferior potting cup (Figure 3A). Anatomical landmarks on the vertebral bodies were digitally registered in the motion capture coordinate system using a probe tool with a 1-mm diameter spherical tip. Motion capture data were acquired at 100 Hz (Optotrak Certus, Northern Digital Inc., Ontario, Canada); the in- and out-of-plane accuracy of this system (bias <0.09°, precision = 0.006°) has previously been quantified by Quarrington et al.[21] Strain gauge and caudal load cell data (MC3A-6-1000, ±4.4 kN, AMTI, Watertown, MA) were acquired at 500 Hz using a data acquisition system (PXIe-1073, BNC-2120 and PXIe-4331 (×2), National Instruments, USA). Loads on the cranial end were measured using the load cell attached to the Hexapod end effector (Omega190, ATI Industrial Automation,

Apex, NC, USA) and were acquired at 10 Hz along with the six leg lengths using the Hexapod data acquisition system. A trigger signal sent to the three independently acquired data streams was used for synchronization.

2.4 | Mechanical testing

Throughout the mechanical testing protocol, all loads and displacements were applied with reference to a rotating coordinate system with its origin fixed at the mechanically prescribed specimen CoR, and the Z (cranial–caudal) and Y (anterior–posterior) axes normal and parallel to the rotating end effector, respectively. The term "axial" refers to loads and displacements applied along the rotating Z-axis. "Constrained flexion" refers to the application of a constant radius flexion rotation (rotation about the negative X axis), *from* a given vertical end effector position, *about* the fixed CoR, with all other axes displacement-constrained.

2.4.1 | Pre-conditioning

The test protocol began with a pre-conditioning sequence to place the specimen in a mechanically stabilized and reproducible state.[31] For the first two specimens, three cycles of constrained flexion, extension, left/right lateral bending, and left/right axial rotation motions (5°, at 0.5–1°/s) were applied. For the remaining specimens, three cycles of constrained flexion rotation (20°, 0.8°/s) from an axial end effector position corresponding to 50 N of compressive
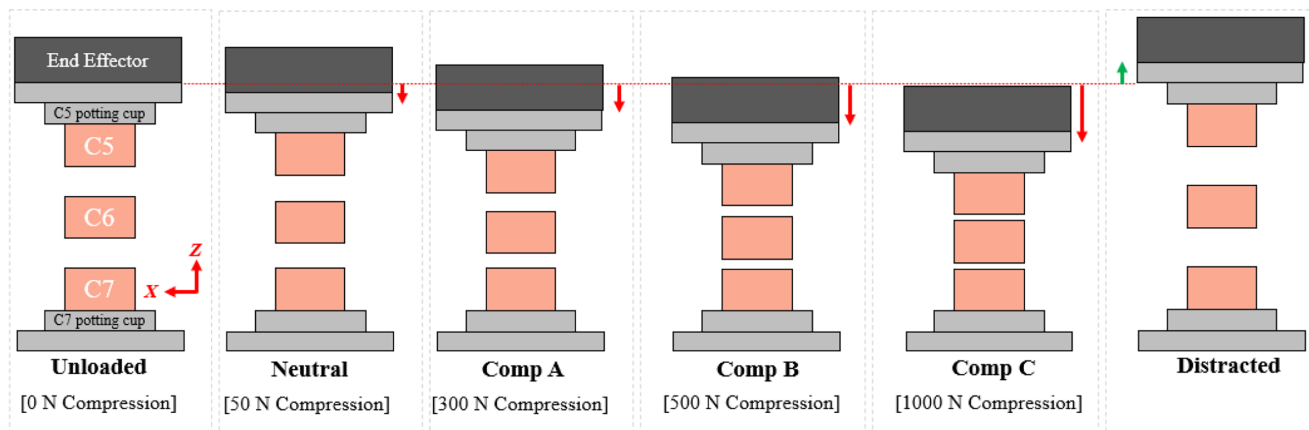
FIGURE 4 Schematic depicting the end effector vertical translation (highlighted by the red and green vertical arrows), as well as the C5/C6 and C6/C7 intervertebral translation required to achieve each of the axial conditions (anterior view). Constrained flexion (rotation about negative X axis) was applied under each axial condition. Images not to scale.

force, were applied. This change in protocol occurred due to technical and logistical constraints and its effect was tested in statistical models.

2.4.2 | Axial condition definition

Immediately following pre-conditioning, with the specimen in 0° flexion, the vertical (Z-axis) position of the hexapod end effector corresponding to each of five axial conditions was determined (Figure 4). The Neutral condition replicated physiological in vivo loading due to the weight of the head, by applying a 50 N axial compressive force (−50 N).[32,33] Three "compressed" conditions representing the spectrum of compressive loading experienced due to neck muscle activation (100–1400 N[32,34–36]) were achieved by applying −300 N (Comp A), −500 N (Comp B), and −1000 N (Comp C). The Distracted condition replicated 2 mm of C6/C7 intervertebral distraction (relative to the Neutral condition), which is similar to that observed by Panjabi et al.[11] during inertially produced CFD in C6/C7 FSUs. To achieve this axial condition, the change in vertical distance between the MC attached to the C6 VB and the MC attached to the C7 potting cup was monitored in real-time, while the robot end effector was moved cranially (+Z), starting from the end effector position corresponding to the Neutral condition.[37] The five axial conditions for each specimen were determined at the start of the testing day (with the specimen in its most hydrated state), and in quick succession. The vertical position of the hexapod end effector which resulted in the force (or intervertebral displacement in the case of the Distracted condition) corresponding to each axial condition at that point in time was recorded. From that point onwards, constrained flexion tests performed in each axial condition were started from the vertical actuator position (and not the axial force, or intervertebral displacement) associated with that axial condition.

Relative to Neutral, an axial end effector translation of −0.58 ± 0.16, −0.78 ± 0.25, −1.40 ± 0.39, and 2.36 ± 0.34 (mean ± 1 standard deviation [SD]; in mm) was required to achieve the Comp A, Comp B, Comp C, and Distracted axial conditions, respectively. As the Neutral axial condition was the reference category for all analyses performed in this study, end effector translations have been reported relative to Neutral, rather than the unloaded position. The C5/C6 and C6/C7 intervertebral translations corresponding to each axial condition are provided in Supporting Information S1.

2.4.3 | Constrained flexion testing

Subsequently, specimens were subjected to three (5/13 specimens) or five cycles of constrained flexion (0°–20°, 0.8°/s), under each of the five axial conditions (3 specimens were not tested in Comp C due to technical challenges, see Supporting Information S2 for details) (Figure 5). The order of application of the Neutral, Comp A, Comp B, and Distracted axial condition was randomized for each specimen, and testing under the Comp C (highest amount of compression) axial condition was conducted last to mitigate against premature specimen damage.

2.4.4 | Pure moment testing

To monitor specimen condition, unconstrained pure moment flexion tests[38–40] were conducted at the start and end of testing (for all specimens), and between constrained flexion testing in each axial condition (for 9/13 specimens) (Figure 6). Pure moment tests were conducted in hybrid control by applying a constant velocity (0.25°/s) flexion rotation up to a flexion moment of 2.5 Nm[41] or a flexion rotation of 24° (maximum range of motion of the testing platform), whichever was achieved first. During pure moment tests, the axial force was maintained at −50 N, and the off-axis shear forces and moments were maintained within ±10 N and ±0.1 Nm, respectively.
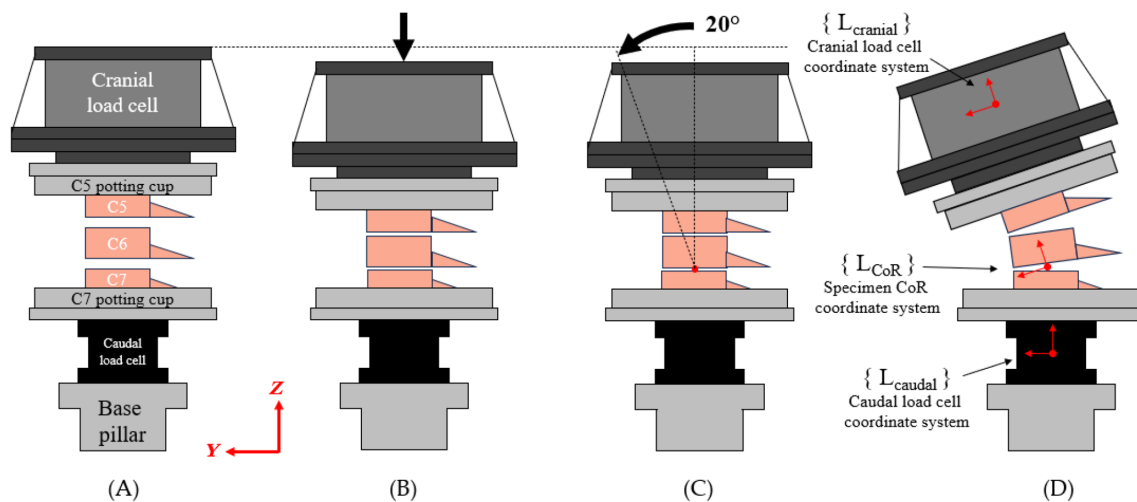
FIGURE 5   Schematic illustrating the key steps for performing a constrained flexion test, using the Comp B axial condition as an example. (A) The specimen in the Neutral axial condition. All data collection is started with the specimen in this condition. (B) The hexapod end effector is moved vertically to the position which was associated with Comp B during the "axial condition definition" step at the start of the testing day. (C) From that position, 20° flexion rotation with constant radius, about the prescribed CoR (center of the C6/C7 disc), is performed. (D) Showing the specimen at 20° flexion, and depicting the coordinate systems at each load cell and at the specimen CoR (red arrows).
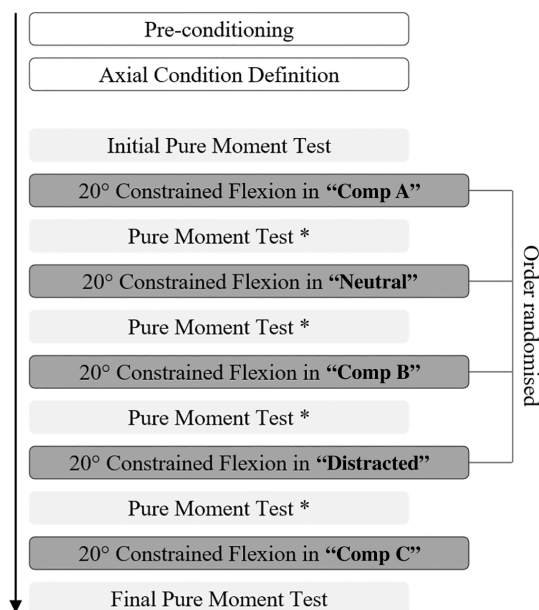

FIGURE 6   Overview of the testing protocol. Order of testing in axial conditions Neutral, Distracted, Comp A, and Comp B, was randomized. The Comp C test was conducted last to mitigate against premature specimen damage. Initial and final pure moment tests were conducted for all specimens, but pure moment tests between the constrained flexion tests (*) were only conducted for 9/13 specimens.

2.5 | Data processing and statistics

CT images were imported into image analysis software (FIJI 2.14.0, ImageJ, MD, USA) to determine the mean VB trabecular volumetric bone mineral density (vBMD) of each specimen. A bone "mask" comprising voxels with Hounsfield Unit (HU) between 150 and 600 HU was created via automated thresholding. An elliptical region of interest (ROI) approximating the total trabecular bone area was placed on at least 10 axial slices per vertebra (C5, C6, and C7) (Supporting Information S3, Figure S1A). The mean HU across all ROIs was converted to the mean VB vBMD using a calibration equation derived from CT images of a calibration phantom (13002, Mindways Software Inc., TX, USA) obtained using the specimen imaging protocol. The AP depth of the C6 superior and inferior endplates at the midsagittal plane were measured manually using RadiAnt DICOM Viewer (2022.1.1, Medixant, Poznan, Poland), and the average of those two measures defined the mean AP VB depth (Supporting Information S3, Figure S1B). The sagittal angle of the bilateral C6/C7 facet joints, defined as the angle of the bilateral inferior C6 facets relative to the inferior C6 endplate, was also measured manually using RadiAnt DICOM Viewer (Supporting Information S3, Figure S1C–F).[42]

Hexapod end effector translations and rotations were calculated from the Hexapod's leg lengths, using custom LabVIEW code which performed the required direct (forward) kinematics.[43] All other data processing was performed using custom MATLAB code (R2018b, Mathworks, MA, USA). The cranial load cell was used to report the loads during constrained flexion testing, and the lower capacity caudal load cell was used for reporting the loads during pure moment testing. All loads were transformed from the respective load cell coordinate system to a coordinate system with its origin at the prescribed CoR and axes that rotate with the hexapod end effector (L_{CoR} in Figure 5D). Load, strain, motion capture marker coordinates, and end effector rotation and translation data, were filtered using a second-order, two-way, low-pass Butterworth filter. A cut-off frequency of 5 Hz was applied to the cranial load data and the end effector rotation and translation data, 10 Hz to the motion capture data, and 100 Hz to the strain gauge and caudal load data.

C5, C6, and C7 VB coordinate systems were defined using the digitally registered anatomical landmarks for each VB. Due to technical challenges experienced with digitally registering anatomical landmarks on the bilateral inferior C6 facets, surrogate coordinate systems were defined using the position data of the three non-collinear infrared emitting diodes on the motion capture MC attached to each facet (refer to Supporting Information S4 for further details). C5/C6 and C6/C7 intervertebral flexion rotations (rotation about the X axis; −ve: flexion of the superior vertebra relative to the inferior), and sagittal angular deflection of the bilateral C6 inferior facets relative to the C6 VB (rotation about the X axis, −ve: deflection of the facet away from the C6 VB, see Supporting Information S5), were calculated by solving for Euler angles using an X–Y–Z (sagittal–coronal–axial) sequence.[44] Principal and shear strains were calculated using the outputs of each rosette strain gauge.

Facet strains and deflections, as well as end effector and intervertebral translations and rotations were zeroed at the start of each test with the specimen at 0° flexion and in the Neutral axial condition. The load cells were zeroed only once at the start of the testing protocol, with the cranial load cell zeroed with nothing attached to it, and the caudal load cell zeroed with the C7 potting cup of the embedded specimen rigidly attached to it. Maximum and minimum principal strain, maximum shear strain, sagittal facet deflection, axial force, flexion moment, and AP shear force at peak flexion in the final test cycle under each axial condition for each specimen were extracted and used in statistical analysis. As data collection for each test began with the specimen in the Neutral axial condition, the outcome measures extracted at peak flexion include the combined effect of applying the axial condition with the specimen at 0° flexion and the subsequent 20° of flexion rotation under that respective axial condition (see Supporting Information S6 for more details).

Statistical analyses were performed using SPSS v24 (IBM, IL, USA). Six linear mixed-effects models (LMMs) were developed to identify if axial condition was associated with the following outcome measures: (1) sagittal facet deflection; (2) maximum shear strain; (3) maximum principal strain; (4) minimum principal strain; (5) flexion moment; (6) axial force; and (7) AP shear force. An a priori main effect of axial condition, and a random effect of facet side nested within donor ID, were included in each model. Shapiro–Wilk and Levene's tests were used to evaluate normality and homogeneity of variance of the dependent variable against the a priori main effect for each model. For each outcome, the effect of the following variables, in the presence of the a priori main effect, was assessed: facet side (left/right), donor age, donor sex, mean VB trabecular vBMD, mean AP VB depth, sagittal angle of the C6/C7 facet joint, test order, and preconditioning method. Adjustment factors that demonstrated some association ($p < 0.25$) with the outcome parameter were included in an initial multivariable model that was iteratively refined using a manual backward step-wise approach until only significant variables, and the a priori main effect, remained ($\alpha = 0.05$). Differences between the three compressed and the Distracted axial conditions relative to Neutral, as well as differences among the three compressed conditions, were evaluated by Bonferroni-adjusted post hoc analyses of the final

multivariable linear mixed-effects models. Unless otherwise stated, descriptive statistics are presented as: mean ± 1 SD and the outcomes of the pairwise post hoc analyses are presented as: estimated mean difference (95% confidence interval [CI]), p-value.

3 | RESULTS

Demographics and geometric measurements for the 13 specimens are provided in Supporting Information S7. The final LMMs are provided in Supporting Information S8.

3.1 | Constrained flexion testing

The sagittal facet deflection, principal and maximum shear strains, flexion moment, and axial and AP shear forces were graphed for all tested specimens. Across all specimens and axial conditions, the C5/C6 and C6/C7 segments accounted for 12.4° ± 3.5° and 8.1° ± 3.6° of the applied 20° of flexion, respectively. In response to three or five cycles of flexion loading, the outcome measures followed a periodic pattern, whereby the magnitude of all outcome measures increased gradually with an increasing amount of flexion rotation. The magnitude of each outcome measure at peak flexion remained consistent across the three or five cycles of applied loading, and the value at peak flexion in the final test cycle under each axial condition was used in all analyses. For brevity, these characteristics are illustrated for only one specimen here (Figure 7A–D).

Axial condition was associated with: sagittal facet deflection when adjusted for test order ($p < 0.001$); maximum principal strain when adjusted for mean AP VB depth and donor sex ($p = 0.006$); maximum shear strain when adjusted for donor age ($p < 0.001$); minimum principal strain ($p < 0.001$); flexion moment when adjusted for mean AP VB depth ($p < 0.001$); axial force when adjusted for potting method and mean AP VB depth ($p < 0.001$); and AP shear force when adjusted for donor sex ($p < 0.001$) (Figures 8 and 9, and Supporting Information S8).

In general, the magnitude of the outcome measures increased as an increasing amount of intervertebral compression (Distracted → Neutral → Comp A → Comp B → Comp C) was superimposed on constrained flexion motions. Sagittal facet deflections were greater in each of the compressed axial conditions compared with Neutral (Comp A vs. Neutral: −0.59° [−1.02, −0.17], $p = 0.006$; Comp B vs. Neutral: −1.21° [−1.63, −0.78], $p < 0.001$; Comp C vs. Neutral: −1.47° [−1.93, −1.00], $p < 0.001$). In the Distracted condition, facet deflections were not appreciable (0.01° ± 0.2°) and were lower than that in the Neutral condition (1.24° [0.82, 1.66], $p < 0.001$).

Compared with the Neutral condition, the magnitude of minimum principal strain was greater in the compressed axial conditions (Comp A vs. Neutral: −126 με [−240, −12], $p = 0.03$; Comp B vs. Neutral: −255 με [−369, −140], $p < 0.001$; Comp C vs. Neutral: −293 με [−417, −169], $p < 0.001$), and lower in the Distracted condition (Distracted vs. Neutral: 202 με [87, 316], $p = 0.001$). Maximum shear
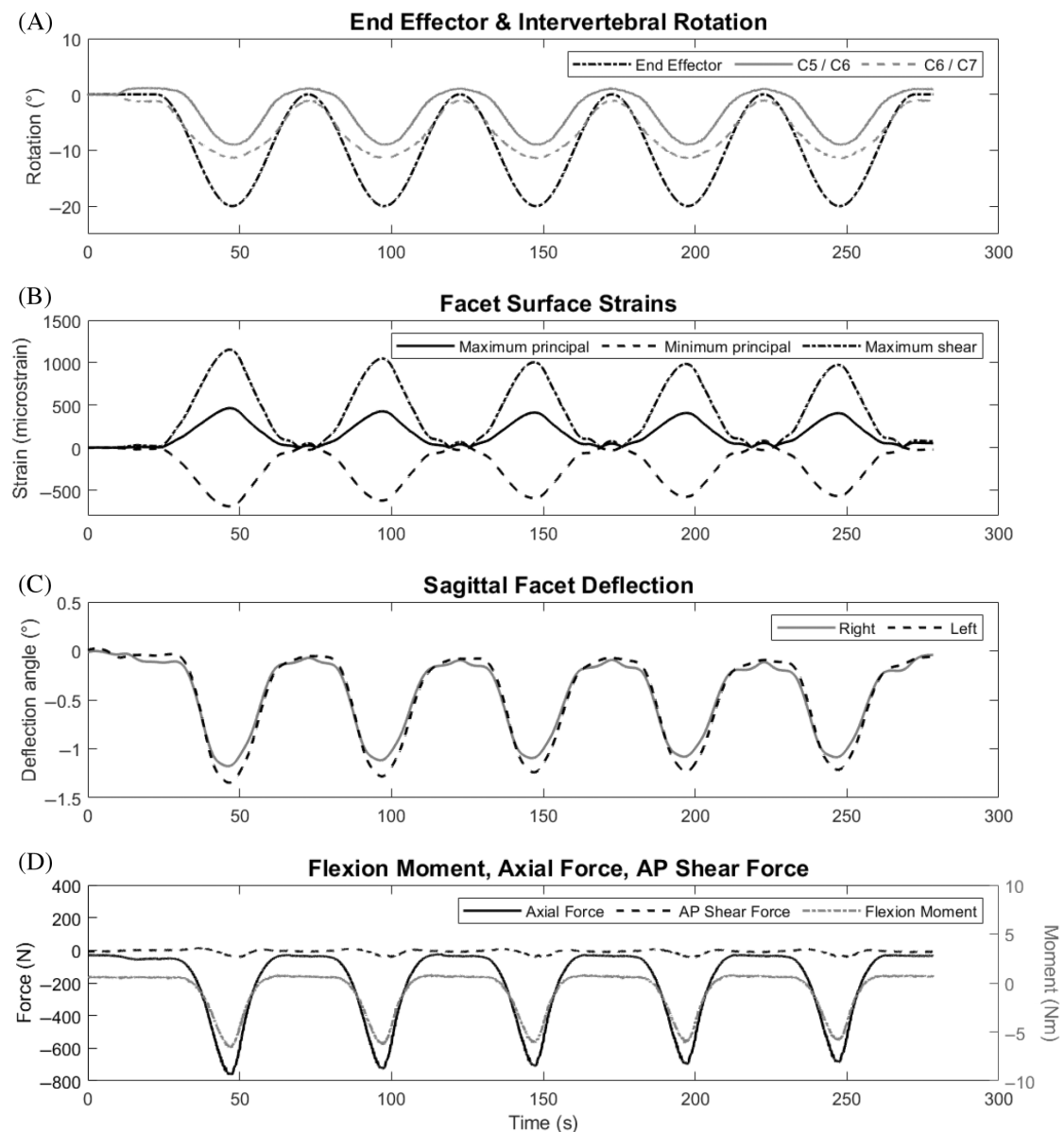
FIGURE 7 Exemplar plot of end effector and intervertebral flexion rotations (A), facet surface strains (right facet only) (B), sagittal facet deflection of the bilateral inferior C6 facets (C), and sagittal plane forces and moments (D), for a single specimen (H01) undergoing five cycles of constrained flexion in the Comp A axial condition. Negative intervertebral rotations indicate flexion of the superior vertebra relative to the inferior vertebra. Negative facet deflections indicate bending of the facet away the C6 VB. As data collection for each test began with the specimen in the Neutral axial condition, the data illustrated here is the change in outcome measure in response to the application of the axial condition with the specimen at 0° flexion (time = 11–23 s), and the subsequent five cycles of 20° flexion rotation.

strain magnitude was higher in Comp B and Comp C relative to Neutral (Comp B vs. Neutral: 366 με [145, 585], $p = 0.001$; Comp C vs. Neutral: 375 με [135, 615], $p = 0.002$), and lower in the Distracted condition (−312 με [−533, −92], $p = 0.006$). There were no differences in maximum principal strain between Neutral and any of the compressed conditions, between Neutral and Distracted, or among any of the compressed conditions.

Peak flexion moment was larger in the Comp B and Comp C conditions and smaller in the Distracted condition, compared with Neutral (Comp B vs. Neutral: −4.31 Nm [−7.80, −0.84], $p = 0.008$; Comp C vs. Neutral: −3.93 Nm [−7.69, −0.11], $p = 0.041$; Distracted

vs. Neutral: 6.29 Nm [2.80, 9.77], $p < 0.001$). Similarly, axial force at peak flexion was larger in the compressed conditions and smaller in Distracted compared with Neutral (Comp A vs. Neutral: −313 N [−482, −143], $p < 0.001$; Comp B vs. Neutral: −608 N [−778, −439], $p < 0.001$; Comp C vs. Neutral: −706 N [−891, −521], $p < 0.001$; Distracted vs. Neutral: 881 N [711, 1051], $p < 0.001$). Finally, AP shear force magnitudes were larger in the Comp B and Comp C and smaller in Distracted compared with Neutral (Comp B vs. Neutral: AP shear force −36 N [−68, −4], $p = 0.025$; Comp C vs. Neutral: AP shear force −55 N [−90, −20], $p = 0.002$; Distracted vs. Neutral: AP shear force 106 N [75, 138], $p < 0.001$).
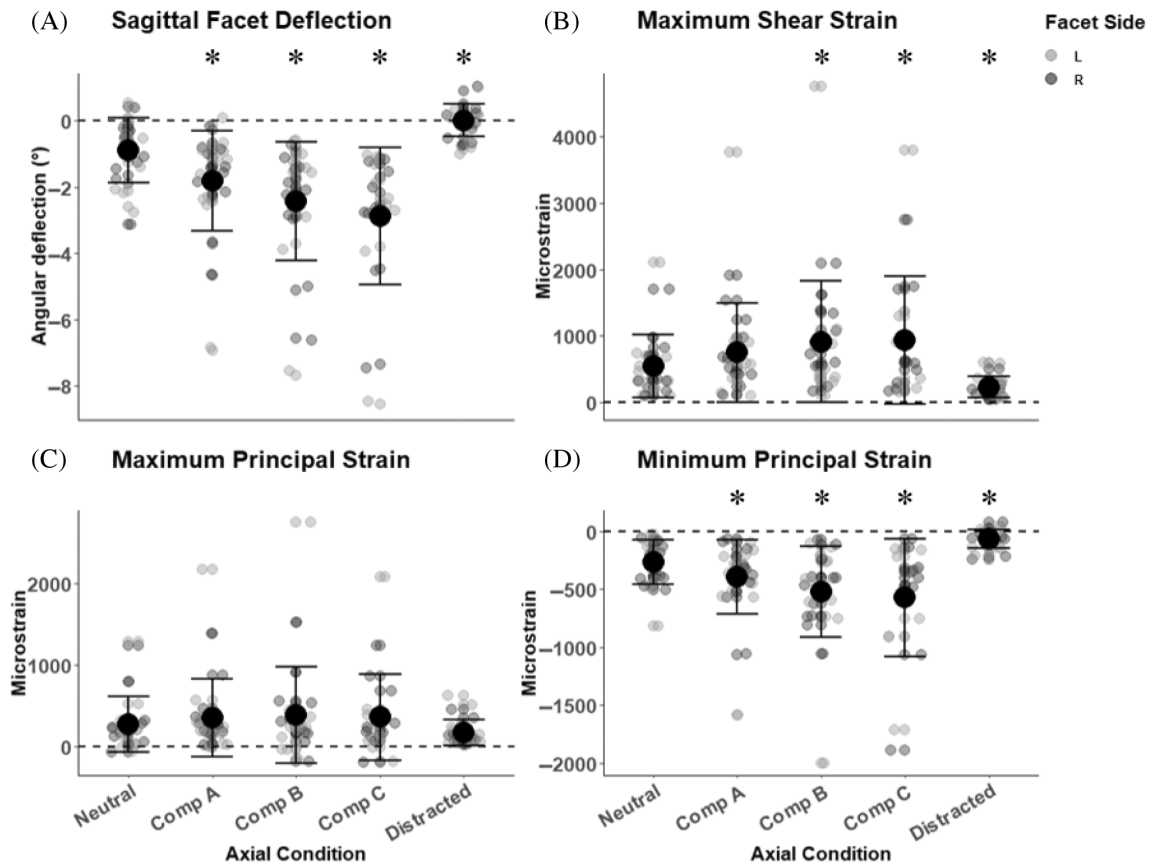
FIGURE 8 Facet surface strains and facet sagittal angular deflection at the peak C5–C7 flexion angle (20°), in each axial condition. Facet surface strains and deflection were not dependent on facet side, hence left and right facet measurements are grouped. Light and gray circles correspond to the value for the left and right facets, respectively, for each specimen. Large black circles and bars are mean ± SD. Significant differences relative to the Neutral axial condition, as determined by Bonferroni-adjusted post hoc analysis of the final multivariable linear mixed-effects models ($\alpha = 0.05$), are indicated on the plots using asterisks.

FIGURE 9 Axial force, flexion moment, and anterior–posterior (AP) shear at the peak C5–C7 flexion angle, in each axial condition. Large black circles and bars are mean ± SD. Significant differences relative to the Neutral axial condition, as determined by Bonferroni-adjusted post hoc analysis of the final multivariable linear mixed-effects models ($\alpha = 0.05$), are indicated on the plots using asterisks.
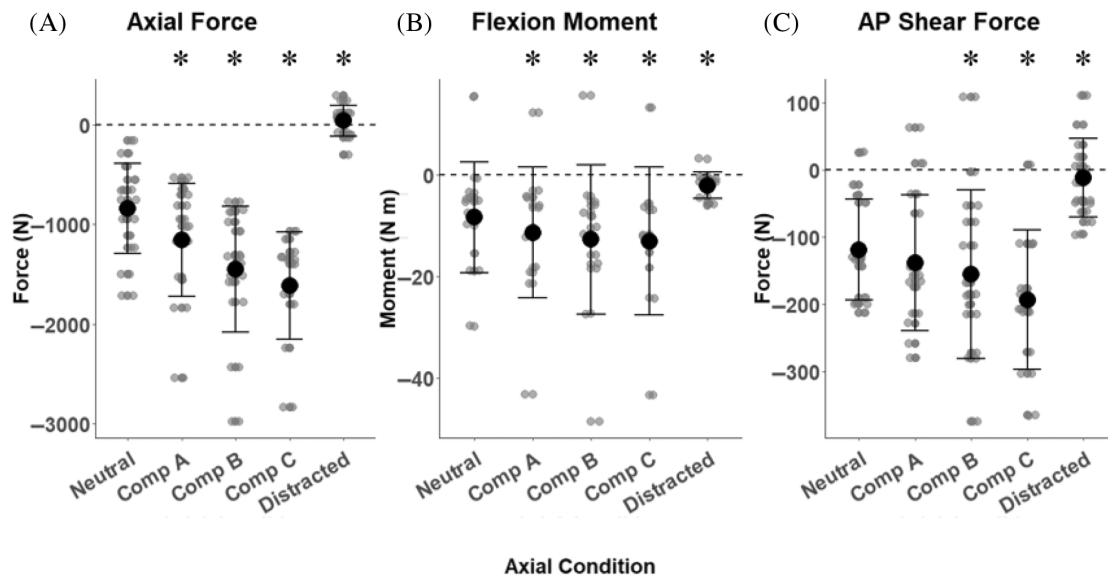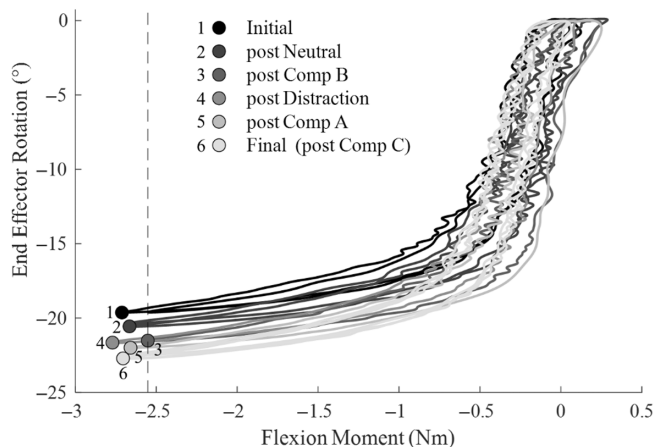
FIGURE 10 Exemplar pure moment test plot for a single specimen (H08). Pure moment tests were conducted at the start and end of the testing suite (i.e., Initial, Final) for all specimens, and in between constrained flexion testing in each axial condition (for 9/13 specimens). The difference in flexion angle between each test was calculated at the greatest flexion moment achieved in all pure moment tests for that specimen. For the depicted specimen, the greatest flexion moment magnitude reached by all pure moment tests was −2.55 Nm (as depicted by the vertical dashed line); the flexion angle for all pure moment tests was extracted at this flexion moment, and differences were calculated.

3.2 | Pure moment testing

The difference in C5–C7 flexion angle between each pure moment test was calculated at the greatest magnitude flexion moment achieved in all pure moment tests for that specimen (Figure 10). Across all specimens, the mean difference in C5–C7 flexion angle between the initial and final pure moment tests was 2.5 ± 1.2° (11% ± 5% of the 20° of applied flexion). For the nine specimens with a complete set of pure moment test data, the mean difference in C5–C7 flexion angle between consecutive pure moment tests (e.g., between post Neutral and post Comp B in Figure 10) was 0.7° ± 0.3° (3% ± 2% of the 20° of applied flexion). The mean duration of the test series was 148 ± 75 min.

4 | DISCUSSION

Facet fractures are frequently associated with clinically observed CFDs; however, to date there has only been one experimental study, using FSUs, which has reported CFD with concomitant facet fracture (CFD + Fx).[21,22] Previous ex vivo studies have suggested two potential mechanisms for CFD injury: *global* eccentric compressive loading applied cranially during simulated head-first impact,[8–10] and *global* distractive-flexion resulting from the weight of the head loading the spine during high deceleration events.[11–15] In vivo, the *intervertebral* compression resulting from the externally applied compressive force and/or neck muscle bracing before head-first impact, or the *intervertebral* distraction associated with the inertial injury mechanism, are

likely to affect the mechanical response of the cervical facets and consequently the likelihood of facet fracture concomitant to CFD. In this study, C5–C7 specimens were subjected to flexion rotation, which is postulated to be the *local* injury vector associated with CFD, under a range of compression and distraction axial conditions. Although the study did not aim to produce fractures, we observed increased facet surface strains and facet deflections with increasing amounts of intervertebral compression (Distracted → Neutral → Comp A → Comp B → Comp C) superimposed on flexion rotations. These data suggest increased facet engagement and higher load transfer through the facet joint, and likely a higher likelihood of facet fracture under the compressed axial conditions compared with the Neutral and Distracted conditions.

Sagittal facet deflections were generally larger in the compressed axial conditions (Comp A, Comp B, and Comp C) and lower in the Distracted condition, relative to Neutral. In the compressed conditions, larger deflections of the bilateral inferior C6 facets *away from* the C6 VB were observed, which is likely to occur due to bony contact between the articulating facets. On the contrary, sagittal facet deflections were either negligible or demonstrated bending *toward* the C6 VB in the Distracted condition, which could be caused by the capsular ligament resisting interfacet separation. Larger facet deflections in the compressed conditions, compared with Distracted and Neutral, were generally accompanied by higher surface strains. Together these outcomes suggest the facets experience greater loading when axial compression (rather than distraction) is superimposed on flexion motions. Increased facet engagement under the compressed axial conditions was also supported by a larger flexion moment, compressive axial force, and anterior shear force at peak flexion.

To date, angular deflections of the cervical facets during physiological or injurious motions have scarcely been reported in the literature. In our laboratory, Quarrington et al.[23] reported sagittal facet deflections of −0.06° ± 0.19°, −0.25° ± 0.18° and −0.19° ± 0.07° in C6/C7 FSUs subjected to 10° of non-destructive flexion superimposed with 50 N of compression (equivalent to Neutral in this study), 300 N of compression (equivalent to Comp A in this study), and intervertebral distraction (defined similarly to Distracted in this study), respectively. Sagittal facet deflections in the Neutral and Distracted conditions were similar between the two studies. However, despite the C6/C7 intervertebral compression required to achieve −300 N (Quarrington et al.[23]: −0.48 ± 0.05 mm; this study: −0.41 ± 0.18 mm), and the applied C6/C7 intervertebral rotation[23] (10°; this study: 8.1° ± 3.6°) being comparable, sagittal facet deflections under the 300 N compression condition (Comp A) were appreciably higher in this study. Despite the boundary condition imposed on the C7 vertebra being similar for the two studies, the different boundary conditions imposed on the C6 vertebra likely affected the loads transferred through the C6/C7 facet joint, and is thought to be the main source of the observed discrepancy.

In this study, the transverse and coronal facet deflections were minimal relative to the sagittal facet deflections (see Supporting Information S9), whereas the transverse facet deflections reported by Quarrington et al.[23] were equal or greater in magnitude to the

corresponding sagittal facet deflections. Variations in the anatomical orientation of the C6/C7 facet joint[45] and the differing boundary conditions imposed on C6 in the two studies are thought to be the primary reasons for the different distribution of the 3D facet deflection among the anatomically relevant planes.

Maximum principal strain and maximum shear strain measured in this study were comparable to those observed at the bilateral inferior C6 facets during constrained flexion testing of FSUs[23] and were substantially larger than those observed during simulated non-destructive flexion loading of isolated sub-axial cervical facets[24] (*maximum principal strain in Neutral*: 256 ± 343 $\mu\varepsilon$ (this study) vs. 336 ± 72 $\mu\varepsilon$[23] vs. 70 ± 8 $\mu\varepsilon$[24]; *maximum shear strain in Neutral*: 520 ± 526 $\mu\varepsilon$ (this study) vs. 712 ± 144 $\mu\varepsilon$[23] vs. 109 ± 15 $\mu\varepsilon$[24]). Minimum principal strains were substantially lower and more variable across specimens in this study compared with previous work (*minimum principal strain in Neutral*: -267 ± 192 $\mu\varepsilon$ (this study) vs. -765 ± 504 $\mu\varepsilon$[23]). Surface strain measurements of bone are highly dependent on the quality and structure of the underlying bone, and on the anatomical location and orientation of the strain gauge. This makes comparison of strain data *between* specimens in this study, as well as with other studies, challenging, as anatomical variability between specimens and precise placement of strain gauges, are likely to contribute to the variations observed in strain readings.

Two specimens (H05 and H11) exhibited facet surface strains greater than two SDs from their respective means in the compressed axial conditions, while the corresponding facet deflections were generally within one SD of the mean (see Supporting Information S10 for further details). Similarly, one specimen (H12) exhibited facet deflections greater than two SDs from the mean, while the corresponding facet surface strains were within one SD of their respective means. The surface strain and facet deflection data for these specimens were not excluded from the analysis because no abnormal facet geometry or bone quality could be identified from their CT images, and no technical issues could be attributed to these observations. Additionally, sagittal facet deflections of $-5.74° \pm 2.31°$, and up to $-14.70°$ at the point of facet fracture have previously been reported under simulated flexion loading in isolated cervical facets[24] and lumbar FSUs,[46] respectively, which are similar in magnitude to the large facet deflections from analyses in this study.

There were several limitations associated with this study. Surface strains and facet deflections were used as an indication of the mechanical response of the cervical facets during constrained flexion; however, preserving the soft tissue structures surrounding the facet joints to ensure biofidelic motion, prevented direct visualization and measurement of interfacet engagement at the C6/C7 cervical facet joints.

Facet response to loading is likely influenced by the presence and extent of facet joint degeneration, and the morphology and bone quality of the articulating facets. In this study, the bilateral facet joints of all specimens were screened for excessive degeneration. However, facet morphology and bone quality were not quantified or included in statistical analyses, primarily because measurement techniques for these parameters are not standardized, and the CT scans lacked

sufficient resolution to accurately estimate trabecular vBMD of the facets. VB AP depth and trabecular vBMD, which are widely-accepted metrics of vertebral size and bone quality, respectively, were included in statistical analyses; however, their relationship to the morphology and bone density of the facets, is not well defined. VB AP depth was the only covariate that consistently remained in the final LMMs; however, with greater sample size the effects of other covariates describing VB and posterior element bone quality and morphology may be assessed. The current study used a repeated measures design, so the contributions of morphology and bone quality to facet response are not likely to alter the within-specimen effects of axial condition that were observed.

Specimens were subjected to constrained flexion, about a fixed CoR. The in vivo instantaneous CoR of cervical motion segments moves anteriorly during flexion rather than being fixed as in this study; however, this anterior translation is minimal for the lower cervical spine motion segments.[29] Applying constrained flexion about a fixed CoR is likely not representative of physiological kinematics; however, during cervical trauma, spinal motion segments likely do not exhibit kinematics within the bounds of "normal" motion, hence quantifying the mechanical response of the cervical facets during constrained motions is still of value.

The quasistatic rotation rate (0.8°/s) was selected to minimize the effect of mechanical system inertia while avoiding creep effects.[41] However, this rate is substantially slower than the rates associated with head-impact loading or inertial loading commonly associated with CFD injuries. The magnitude of facet deflections and strains reported in this study may differ from a dynamic testing environment; however, the relative effect of axial condition on the mechanical response of the cervical facets is likely to still exist at higher rates of loading.

The testing platform used for this study could apply 20°–24° of flexion rotation, which limited this study to non-destructive testing of two motion segment specimens. Two motion segment C5–C7 specimens were selected because CFDs most frequently occur at C5/C6 and C6/C7,[3,7] and the sum of the physiologic intervertebral range of motion of C5/C6 (9.3° ± 3.3°) and C6/C7 (9.3° ± 3.5°)[47] in flexion could be achieved in the test platform. Future investigations using head–neck specimens or whole cadavers, may further elaborate the role of intervertebral compression and distraction superimposed on *global* motions associated with CFD (compression or distractive flexion) on the mechanical response of the cervical facets.

The pre-conditioning protocol differed among specimens tested in this study, but this parameter was not a significant covariate in any of the LMMs. Specimens were also subjected to a variable number of testing cycles, due to variable cycles of constrained flexion testing (3 cycles per axial condition in 5 specimens; 5 cycles per axial condition in 8 specimens), and pure moment tests between constrained flexion tests being performed on 9/13 specimens. Variation in total testing cycles could potentially cause inconsistency in tissue putrefaction and soft tissue relaxation, and affect the biomechanical response of specimens. However, pure moment tests conducted at the start and end of the test series for each specimen demonstrated a 2.5°

± 1.2° increase in C5–C7 flexion range of motion (11% ± 5% of the 20° of applied flexion) at an equivalent applied flexion moment, which is similar to that reported in previous studies.[31,48] No specimen had a substantially larger increase in ROM than the remainder of the cohort. These outcomes suggest that the variation in total testing cycles among specimens likely had minimal effect on the outcome measures.

To minimize the potential biomechanical effects of soft tissue relaxation and incipient tissue putrefaction over the duration of the test series (148 ± 75 min) on the study outcomes, the order of testing in each axial condition (except Comp C) was randomized. Due to the use of line-of-sight motion capture and strain gauges, specimens could not be immersed in a fluid bath or wrapped in gauze or plastic film during testing, but specimen hydration was maintained using PBS spray. The effect of soft tissue relaxation and incipient tissue putrefaction on the definition of the axial conditions was minimized by identifying the specimen-specific actuator positions corresponding to each axial condition, in quick succession, at the commencement of testing.

In conclusion, increasing amounts of intervertebral compression superimposed on constrained flexion rotations applied to C5–C7 specimens were associated with an increase in the magnitude of facet surface strains and facet deflections of the C6 inferior facet. This suggests increased facet engagement, higher load being transferred through the facet joint, and a potentially higher likelihood of facet fracture under the compressed axial conditions compared with Neutral and Distracted. Further experimental work using multi-segment cervical spine specimens and full head–neck specimens at quasistatic and dynamic rates will provide a more complete understanding of the *local* and *global* loading mechanisms most likely to result in CFD with concomitant facet fracture.

AUTHOR CONTRIBUTIONS

Parham Foroutan, Claire F. Jones, Ryan D. Quarrington, John J. Costi, and Peter A. Cripton conceived of, and designed, this study. Parham Foroutan, Ryan D. Quarrington, Boyin Ding, and Michael P. Russo performed the experiments. Parham Foroutan performed the data analysis, and drafted the manuscript. Claire F. Jones and John J. Costi, Cripton supervised the work. Ryan D. Quarrington, Claire F. Jones, John J. Costi, and Peter A. Cripton assisted interpretation of data. Claire F. Jones, Ryan D. Quarrington, John J. Costi, Boyin Ding, Michael P. Russo, and Peter A. Cripton provided critical revision of the manuscript.

CONFLICT OF INTEREST STATEMENT

The authors declare that no benefits in any form have been or will be received from a commercial party related directly or indirectly to the subject of this manuscript.

ORCID

Parham Foroutan https://orcid.org/0000-0002-0510-8518
Ryan D. Quarrington https://orcid.org/0000-0002-0633-2482
Michael Pyrros Russo https://orcid.org/0000-0002-4784-0539
Boyin Ding https://orcid.org/0000-0001-8417-8057
Peter A. Cripton https://orcid.org/0000-0002-5067-0833
John J. Costi https://orcid.org/0000-0002-8267-7837
Claire F. Jones https://orcid.org/0000-0002-0995-1182

REFERENCES

1. Vaccaro AR, Koerner JD, Radcliff KE, et al. AOSpine subaxial cervical spine injury classification system. *Eur Spine J*. 2016;25(7):2173-2184.
2. Hadley MN, Fitzpatrick BC, Sonntag VK, Browner CM. Facet fracture-dislocation injuries of the cervical spine. *Neurosurgery*. 1992;30(5):661-666.
3. Quarrington RD, Jones CF, Tcherveniakov P, et al. Traumatic subaxial cervical facet subluxation and dislocation: epidemiology, radiographic analyses, and risk factors for spinal cord injury. *Spine J*. 2018;18(3):387-398.
4. Khezri N, Ailon T, Kwon BK. Treatment of facet injuries in the cervical spine. *Neurosurg Clin*. 2017;28(1):125-137.
5. Dvorak MF, Fisher CG, Aarabi B, et al. Clinical outcomes of 90 isolated unilateral facet fractures, subluxations, and dislocations treated surgically and nonoperatively. *Spine*. 2007;32(26):3007-3013.
6. Bohlman HH. Acute fractures and dislocations of the cervical spine. An analysis of three hundred hospitalized patients and review of the literature. *J Bone Joint Surg Am*. 1979;61(8):1119-1142.
7. Anissipour AK, Agel J, Bellabarba C, Bransford RJ. Cervical facet dislocations in the adolescent population: a report of 21 cases at a Level 1 trauma center from 2004 to 2014. *Eur Spine J*. 2017;26(4):1266-1271.
8. Bauze RJ, Ardran GM. Experimental production of forward dislocation in the human cervical spine. *J Bone Joint Surg*. 1978;60(2):239-245.
9. Pintar FA, Yoganandan N, Sances A, Reinartz J, Harris G, Larson SJ. Kinematic and anatomical analysis of the human cervical spinal column under axial loading. *SAE Trans*. 1989;98:1766-1789.
10. Yoganandan N, Sances A, Maiman DJ, Myklebust JB, Pech P, Larson SJ. Experimental spinal injuries with vertical impact. *Spine*. 1986;11(9):855-860.
11. Panjabi MM, Simpson AK, Ivancic PC, Pearson AM, Tominaga Y, Yue JJ. Cervical facet joint kinematics during bilateral facet dislocation. *Eur Spine J*. 2007;16(10):1680-1688.
12. Ivancic PC, Pearson AM, Tominaga Y, Simpson AK, Yue JJ, Panjabi MM. Biomechanics of cervical facet dislocation. *Traffic Inj Prev*. 2008;9(6):606-611.
13. Ivancic PC, Pearson AM, Tominaga Y, Simpson AK, Yue JJ, Panjabi MM. Mechanism of cervical spinal cord injury during bilateral facet dislocation. *Spine*. 2007;32(22):2467-2473.
14. Forman J, Lopez-Valdes F, Lessley D, et al. Rear seat occupant safety: an investigation of a progressive force-limiting, pretensioning 3-point

belt system using adult PMHS in frontal sled tests. *Stapp Car Crash J.* 2009;53:49.

15. Huelke DF, Mackay GM, Morris A, Bradford M. A review of cervical fractures and fracture-dislocations without head impacts sustained by restrained occupants. *Accid Anal Prev.* 1993;25(6):731-743.

16. Nightingale RW, McElhaney JH, Camacho DL, Kleinberger M, Winkelstein BA, Myers BS. *The Dynamic Responses of the Cervical Spine: Buckling, End Conditions, and Tolerance in Compressive Impacts.* SAE Technical Paper; 1997.

17. Swartz EE, Floyd R, Cendoma M. Cervical spine functional anatomy and the biomechanics of injury due to compressive loading. *J Athl Train.* 2005;40(3):155.

18. Iencean S. Classification of spinal injuries based on the essential traumatic spinal mechanisms. *Spinal Cord.* 2003;41(7):385-396.

19. Hodgson VR, Thomas LM. Mechanisms of cervical spine injury during impact to the protected head. *SAE Trans.* 1980;89:3792-3805.

20. Ivancic PC. Head-first impact with head protrusion causes noncontiguous injuries of the cadaveric cervical spine. *Clin J Sport Med.* 2012; 22(5):390-396.

21. Quarrington RD, Costi JJ, Freeman BJC, Jones CF. Investigating the effect of axial compression and distraction on cervical facet mechanics during supraphysiologic anterior shear. *J Biomech Eng.* 2021; 143(6):061014.

22. Foster JB, Kerrigan JR, Nightingale RW, et al. Analysis of cervical spine injuries and mechanisms for CIREN rollover crashes. In: International Research Council on the Biomechanics of Injury Conference. 2012.

23. Quarrington RD, Costi JJ, Freeman BJC, Jones CF. The effect of axial compression and distraction on cervical facet mechanics during anterior shear, flexion, axial rotation, and lateral bending motions. *J Biomech.* 2019;83:205-213.

24. Quarrington RD, Costi JJ, Freeman BJC, Jones CF. Quantitative evaluation of facet deflection, stiffness, strain and failure load during simulated cervical spine trauma. *J Biomech.* 2018;72:116-124.

25. Cripton PA. *Load-Sharing in the Human Cervical Spine.* Queen's University; 2000.

26. Nightingale RW, Sganga J, Cutcliffe H, Bass CR. Impact responses of the cervical spine: a computational study of the effects of muscle activity, torso constraint, and pre-flexion. *J Biomech.* 2016;49(4): 558-564.

27. Dvorak J, Froehlich D, Penning L, Baumgartner H, Panjabi MM. Functional radiographic diagnosis of the cervical spine: flexion/extension. *Spine.* 1988;13(7):748-755.

28. Van Mameren H, Sanches H, Beursgens J, Drukker J. Cervical spine motion in the sagittal plane II: position of segmental averaged instantaneous centers of rotation-a cineradiographic study. *Spine.* 1992; 17(5):467-474.

29. Anderst W, Baillargeon E, Donaldson W, Lee J, Kang J. Motion path of the instant center of rotation in the cervical spine during in vivo dynamic flexion-extension: implications for artificial disc design and evaluation of motion quality following arthrodesis. *Spine.* 2013; 38(10):E594-E601.

30. Ding B. *A Study of a Gough-Stewart Platform-Based Manipulator for Applications in Biomechanical Testing.* University of Adelaide; 2014.

31. Costi JJ, Ledet EH, O'Connell GD. Spine biomechanical testing methodologies: the controversy of consensus vs scientific evidence. *JOR Spine.* 2021;4(1):e1138.

32. Bell KM, Yan Y, Debski RE, Sowa GA, Kang JD, Tashman S. Influence of varying compressive loading methods on physiologic motion patterns in the cervical spine. *J Biomech.* 2016;49(2):167-172.

33. DiAngelo DJ, Foley KT. An improved biomechanical testing protocol for evaluating spinal arthroplasty and motion preservation devices in a multilevel human cadaveric cervical model. *Neurosurg Focus.* 2004; 17(3):1-29.

34. Chancey VC, Nightingale RW, van Ee C, Knaub KE, Myers BS. Improved estimation of human neck tensile tolerance: reducing the range of reported tolerance using anthropometrically correct muscles and optimized physiologic initial conditions. *Stapp Car Crash J.* 2003; 47:135-153.

35. Newell RS, Siegmund GP, Blouin JS, Street J, Cripton PA. Cervical vertebral realignment when voluntarily adopting a protective neck posture. *Spine.* 2014;39(15):E885-E893.

36. Hattori S. Cervical intradiscal pressure in movements and traction of the cervical spine. *Z Orthop Ihre Grenzgeb.* 1981;119:568-569.

37. Derzsi Z, Volcic R. MOTOM toolbox: MOtion tracking via Optotrak and Matlab. *J Neurosci Methods.* 2018;308:129-134.

38. Goertzen DJ, Lane C, Oxland TR. Neutral zone and range of motion in the spine are greater with stepwise loading than with a continuous loading protocol. an in vitro porcine investigation. *J Biomech.* 2004; 37(2):257-261.

39. Schulze M, Hartensuer R, Gehweiler D, Hölscher U, Raschke MJ, Vordemvenne T. Evaluation of a robot-assisted testing system for multisegmental spine specimens. *J Biomech.* 2012;45(8):1457-1462.

40. Lysack JT, Dickey JP, Dumas GA, Yen D. A continuous pure moment loading apparatus for biomechanical testing of multi-segment spine specimens. *J Biomech.* 2000;33(6):765-770.

41. Wilke H-J, Wenger K, Claes LJ. Testing criteria for spinal implants: recommendations for the standardization of in vitro stability testing of spinal implants. *Eur Spine J.* 1998;7(2):148-154.

42. Takao T, Kubota K, Maeda T, et al. A radiographic evaluation of facet sagittal angle in cervical spinal cord injury without major fracture or dislocation. *Spinal Cord.* 2017;55(5):515-517.

43. Faügère J-C, Merlet J-P, Rouillier F. *On Solving the Direct Kinematics Problem for Parallel Robots.* INRIA; 2006.

44. Robertson DGE, Caldwell G, Hamill J, Kamen G, Whittlesey S. *Research Methods in Biomechanics.* 2nd ed. Human Kinetics; 2013.

45. Pal G, Routal R, Saggu S. The orientation of the articular facets of the zygapophyseal joints at the cervical and upper thoracic region. *J Anat.* 2001;198(4):431-441.

46. Green TP, Allvey JC, Adams MA. Spondylolysis: bending of the inferior articular processes of lumbar vertebrae during simulated spinal movements. *Spine.* 1994;19(23):2683-2691.

47. Anderst W, Donaldson WF, Lee JY, Kang JD. Three-dimensional intervertebral kinematics in the healthy young adult cervical spine during dynamic functional loading. *J Biomech.* 2015;48(7):1286-1293.

48. Wilke HJ, Jungkunz B, Wenger K, Claes LE. Spinal segment range of motion as a function of in vitro test conditions: effects of exposure period, accumulated cycles, angular-deformation rate, and moisture condition. *Anat Rec.* 1998;251(1):15-19.

SUPPORTING INFORMATION

Additional supporting information can be found online in the Supporting Information section at the end of this article.